ISSN 1070-3284, Russian Journal of Coordination Chemistry, 2018, Vol. 44, No. 4, pp. 284–300. © Pleiades Publishing, Ltd., 2018.
Original Russian Text © M.A. Katkova, 2018, published in Koordinatsionnaya Khimiya, 2018, Vol. 44, No. 2, pp. 135–150.

Water-Soluble Polynuclear Metallamacrocyclic Copper(II) and Lanthanide(III) Complexes Based on Amino Hydroxamic Acids

M. A. Katkova

Razuvaev Institute of Organometallic Chemistry, Russian Academy of Sciences, Nizhny Novgorod, 603950 Russia
e-mail: marina@iomc.ras.ru

Received September 15, 2017

Abstract—Data on the synthesis and structure of water-soluble polynuclear copper(II) and lanthanide(III) metallamacrocycles based on amino hydroxamic acids are presented. The structural features of the obtained 15-MC-5 metallacrown aqua complexes and their applicability as NMR contrast agents are considered. Additionally, the applicability as molecular precursors for the synthesis of nano-sized materials was demonstrated for Ce(III) compounds.

Keywords: water-soluble polynuclear metallamacrocyclic complexes, transition metals, lanthanides, amino hydroxamic acids

DOI: 10.1134/S107032841804005X

INTRODUCTION

The interest in the metal compounds with nitrogen-containing biologically active ligands is constantly increasing. Hydroxamic acids RCC(O)-N(RN)OH, which have been known since 1869, are currently systematically and widely studied as the active components of siderophores, which play a considerable role in biochemical processes as inhibitors of certain enzymes, providing anticancer properties, and they are also used for lanthanide preconcentration and extraction [1, 2]. Amino hydroxamic acid derivatives form a new, rapidly developing line of research related to increase in the denticity of hydroxamic acids as a result of introduction of an additional amino group.

α-Amino hydroxamic acids (NH_2–CHR–CO–NH–OH), known for the broad spectrum of biological activities, are efficient N,N- and O,O-type chelating ligands. A distinctive feature of chelate complexes based on amino hydroxamic acids is the diversity of resulting structures depending on the nature of the metal [3, 4]. The *d*-metals present in biological molecules are most important. Copper is an essential element for the vital activity of animals and plants: it occurs in copper-containing proteins and enzymes, which play an important role in acceleration of metabolic processes and enhancement of tissue respiration, and participates in growth and reproduction processes [5]. In recent years, particular interest was aroused in polynuclear heterometallic compounds containing simultaneously copper and lanthanide ions [6–9].

Polynuclear metallamacrocyclic compounds, which were first described by the American research team headed by Professor Pecoraro in 1989, represent a unique class of supramolecular compounds structurally resembling crown ethers [10]. The trivial names of these compounds are formed by analogy with crown ether names. For example, in 15-MC-5, the number 15 designates the number of atoms in the ring, MC is the class of compounds (metallacrown), and 5 is the number of electron-donating O atoms (Fig. 1). The generally accepted names are MX[ringsize-MC_{M*L}-ringoxygen]Y, where M is the central atom, X is an anion coordinated to the central atom, M* is the ring metal atom, L is the organic ligand, and Y is the nonbonded anion [7]. Our investigations were concerned with Cu(II)–Ln(III) polynuclear metallamacrocyclic compounds 15-MC-5 based on amino hydroxamic acids.

FORMATION OF POLYNUCLEAR COPPER(II) AND LANTHANIDE(III) METALLAMACROCYCLIC COMPOUNDS

The synthesis of polynuclear Cu(II)-Ln(III) 15-MC-5 metallamacrocycles is very simple. It is only necessary to mix lanthanide nitrate, copper acetate, and amino hydroxamic acid to observe dark blue coloring inherent in Cu(II)-Ln(III) metallacrowns. One of the first metallacrowns, $Eu(NO_3)$[15-$MC_{Cu(II)Glyha}$-5]$(NO_3)_2$ (**I**), was synthesized by Pecoraro in 1999 (Fig. 2a) [11].

A specific structural feature of complex **I** is the presence of a planar metallamacrocycle composed of five Cu^{2+} ions, five glycine hydroxamate ligands, and the Eu^{3+} central atom coordinated to five oxygen atoms of the ring (Fig. 2a). This structure provides a

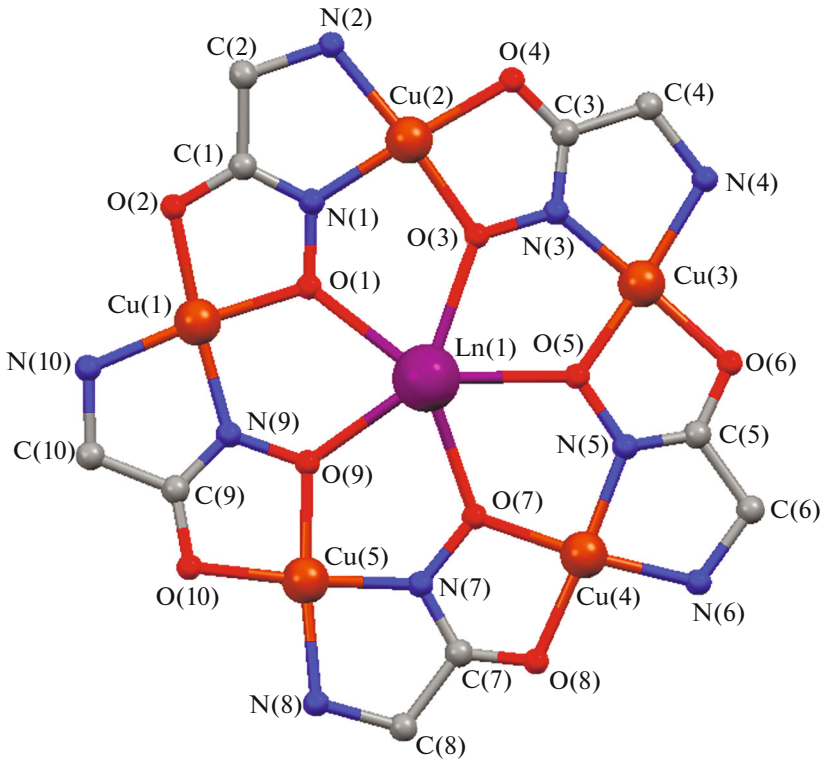

Fig. 1. Structure of metallacrown 15-MC-5 based on glycine hydroxamic acid.

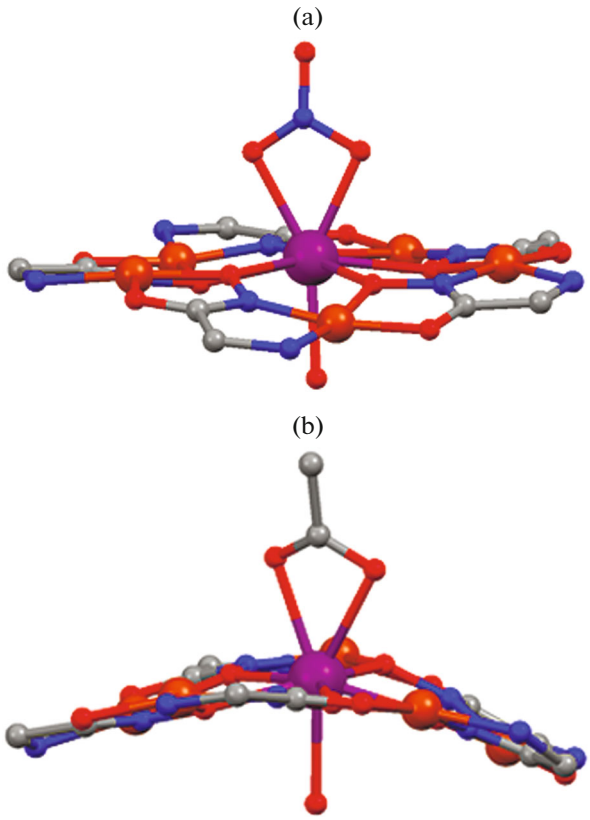

Fig. 2. Molecular structures of complexes (a) **I** [11] and (b) **II**. The hydrogen atoms are omitted.

potential possibility for the axial coordination of additional ligands to the lanthanide ion. It is known that lanthanide ions in polynuclear complexes have coordination numbers of 8–10. In complex **I**, the Eu(III) coordination number of 8 (one-cap pentagonal bipyramid) is attained via coordination to three O atoms of the bidentate NO_3 group and to a water molecule. It is evident that these apical ligands can be varied as a result of competition between ligands and other donor molecules or ions present in the reaction system.

Despite the previously reported data, indicating that the acetate ion cannot be coordinated to a lanthanide in the presence of the NO_3^- anion [7–9, 12–16], we have synthesized for the first time the complex $Eu(OOCCH_3)[15\text{-}MC_{Cu(II)Glyha}\text{-}5](NO_3)_2$ (**II**), in which the acetate ion is coordinated to Eu in the bidentate fashion, while the nitrate anions are not bound to europium [17] (Fig. 2b).

In the synthesis of complex **II**, it was useful to add Ca(II) salts, in particular, calcium acetate in the case of $Eu(NO_3)_3$ used as the starting reactant or calcium nitrate in the case of $EuCl_3$. According to X-ray diffraction data, compounds **I** and **II** have similar structure (Table 1). The Eu–O distances differ somewhat depending on the nature of the apical ligand. For instance, the Eu–O(Ac) distance in complex **II** increases, on average, to 2.492 Å, while the average value for the Eu–O(NO_3) complex **I** is 2.381 Å.

Table 1. Selected bond lengths (Å) and angles (deg) in compounds **I** and **II**

Bonds and angles	*d*, Å and ω, deg	
	I [11]	**II**
Cu–Eu	3.890–3.911	3.852 (4)–3.905(4)
Cu–Cu	4.575–4.589	4.566(5)–4.607(5)
$Eu–O_{oxime}$	2.406– 2.493	2.406(2)–2.443(2)
$Cu–O_{oxime}$	1.902–1.946	1.935(2)–1.965(2)
$Cu–O_{carbonyl}$	1.943–1.972	1.938(2)–1.968(2)
$Cu–N_{imine}$	1.887–1.919	1.902(3)–1.917(3)
$Cu–N_{amine}$	1.990–2.022	2.006(2)–2.041(2)
$Cu–O_{aq}$	2.400–2.463	2.300(3)–2.496(3)
$Eu–O_{(acetate\ or\ NO_3)}$	2.369–2.392	2.470(4)–2.515(2)
$Eu–O_{aq}$	2.392	2.439(2)
Cavity radius	1.14	1.06
$CuO_{oxime}Eu$	123.4–125.7	123.56(8)–126.67(9)
$O_{oxime}EuO_{oxime}$	70.6–72.7	70.32(7)–74.00(6)

The 15-MC-5 ring of **II** has a non-planar shape resembling a bowl with the Eu^{3+} ion at the centre. In the case of acetate anion, the geometry of the ring of **II** is markedly distorted as compared with that of **I**, in which the NO_3 anion is present. Probably, this is attributable to the presence of intermolecular hydrogen bonds (Fig. 3).

The mild conditions of the synthesis that we developed (room temperature, one-step & one-pot reaction in water, presence of calcium salts) allowed us to selectively obtain water-soluble Cu(II)-Ln(III) 15-MC-5 based on glycine hydroxamate with various axial ligands (Fig. 4) [18].

X-ray diffraction analysis was carried out for $Nd(NO_3)[15\text{-}MC_{Cu(II)Glyha}\text{-}5](NO_3)_2$ (**III**), $Y(OAc)\text{-}[15\text{-}MC_{Cu(II)Glyha}\text{-}5](NO_3)_2$ (**IV**), $La(NO_3)[15\text{-}MC_{Cu(II)Glyha}\text{-}5](NO_3)_2$ (**V**), and $Gd(lactate)[15\text{-}MC_{Cu(II)Glyha}\text{-}5](Cl)_2$ (**VI**) (Table 2).

The data of Tables 1 and 2 indicate that the geometric characteristics of the metallamacrocycles consisting of five [Cu(II)-N-O]-hydroxamate repeating units around the central lanthanide ion are similar for

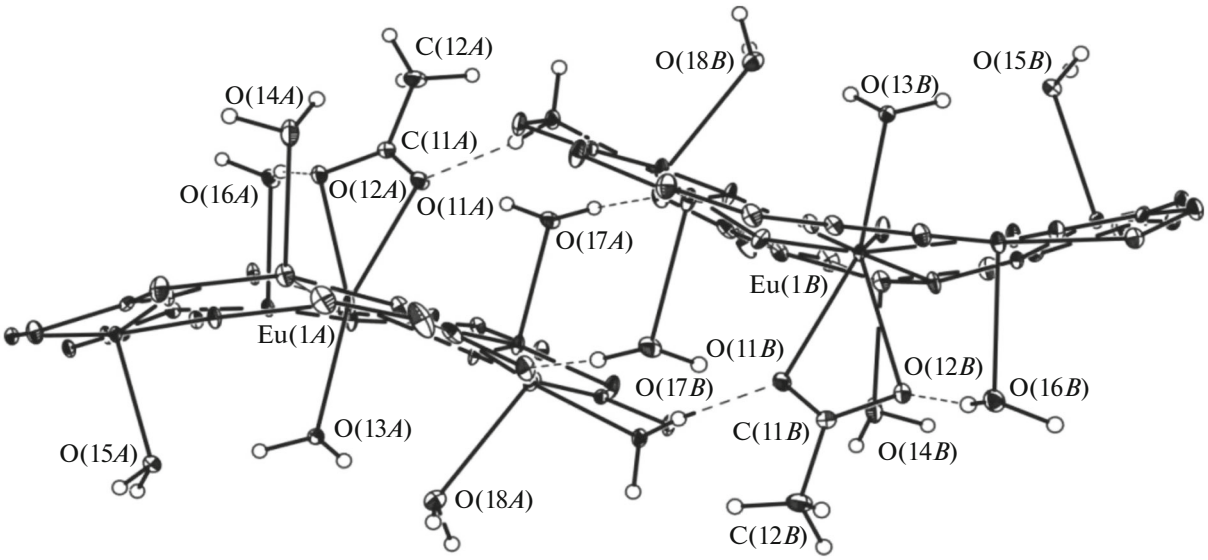

Fig. 3. Fragment of the packing of complex **II**.

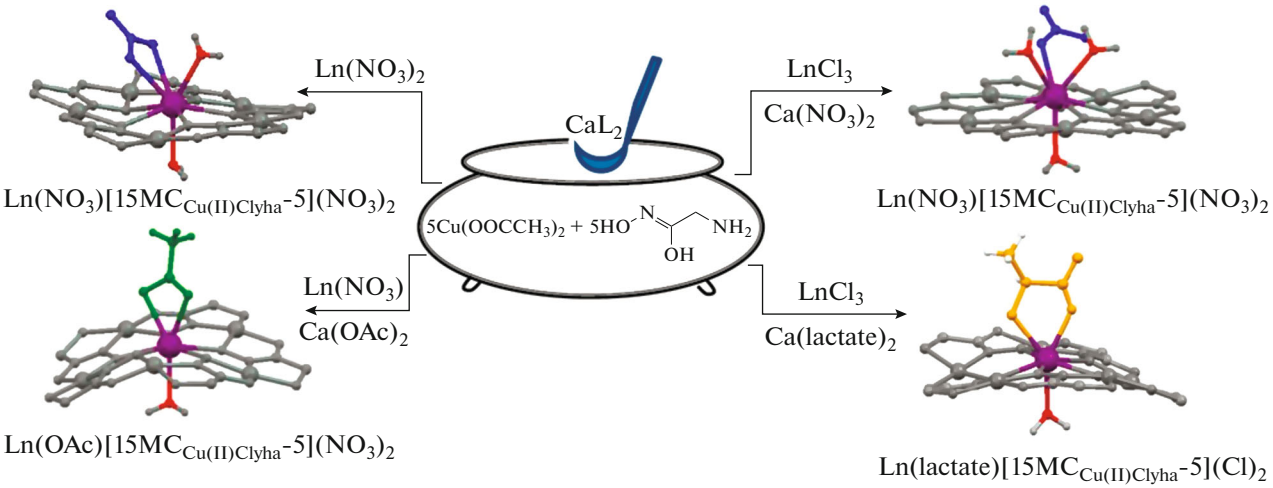

Fig. 4. Scheme of the synthesis of Cu(II)-Ln(III) 15-MC-5 compounds with various axial ligands.

structures **I**–**VI**. A structure distortion can be induced by additional coordination of O-donor apical ligands. For example, in complex **III**, the Nd(III) atom is nine-coordinated with additional coordination of the bidentate nitrate ion and two water molecules (Fig. 5a). The deviation of non-hydrogen atoms of the 15-$MC_{Cu(II)Glyha}$-5 ring from the plane is 0.22 Å. The Nd^{3+} ion is displaced from the plane by 0.2630(2) Å towards the bidentate nitrate group. In complex **IV**, the coordination number of the central Y(III) atom is 8. Apart from the five hydroxamate oxygen atoms, the Y coordination sphere contains oxygen atoms of the bidentate acetate ion and one water molecule located on different sides of the ring (Fig. 5b). The non-planar ring has a dome shape, with the convex side facing the acetate ion. The deviation of non-hydrogen atoms of the 15-$MC_{Cu(II)Glyha}$-5 ring from the plane is 0.51 Å. In complex **V**, the central La(III) atom has a coordination number of 9 (Fig. 5c). The 15-$MC_{Cu(II)Glyha}$-5 ring ring is almost planar, the non-hydrogen atoms deviate from the ring plane by 0.12 Å. The La atom is displaced from the ring plane by 0.6110(5) Å towards the nitrate O atom. The nitrate ion forms a bridge between the La^{3+} and Cu^{2+} ions. In complex **VI**, the coordination number of (Gd(III)) is 8. The metallamacrocyclic moiety is dome-shaped with the convex side facing the lactate ion. The Gd(III)–$O_{lactate}$ distances are 2.32(1) and 2.46(1) Å (Fig. 5d).

Table 2. Comparison of structural parameters for **III**–**VI**

Bonds and angles	*d*, Å and ω, deg			
	III (Ln = Nd)	**IV** (Ln = Y)	**V** (Ln = La)	**VI** (Ln = Gd)
Cu–Ln	3.8667(2)–3.9655(2)	3.826(1)–3.884(1)	3.9030(4)–3.9814(4)	3.856(2)–3.900(2)
Cu–Cu	4.5871(3)–4.6045(3)	4.556(1)–4.590(1)	4.5725(5)–4.5958(5)	4.543(2)–4.673(4)
Ln–O_{oxime}	2.438(1)–2.521(1)	2.372(5)–2.410(5)	2.521(2)–2.584(2)	2.387(9)–2.437(8)
Cu–O_{oxime}	1.922(1)–1.949(1)	1.935(5)–1.976(6)	1.907(2)–1.930(2)	1.927(9)–1.938(9)
Cu–$O_{carbonyl}$	1.938(1)–1.955(1)	1.924(6)–1.966(6)	1.937(2)–1.950(2)	1.92(1)–1.95(1)
Cu–N_{imine}	1.901(1)–1.915(1)	1.893(7)–1.911(7)	1.902(3)–1.912(3)	1.90(1)–1.99(1)
Cu–N_{amine}	1.998(1)–2.034(1)	2.008(7)–2.039(7)	1.989(3)–2.014(2)	2.00(1)–2.04(3)
Ln–O_{aq}	2.447(1), 2.463(1)	2.368(5)	2.561(2)–2.586(2)	2.390(9)
Ln–O_{ligand}	2.623(1), 2.796(1)[a]	2.43(1), 2.462(6)[b]	2.588(2)[a]	2.32(1), 2.46(1)[c]
$O_{oxime}CuN_{imine}$	90.01(5)–92.17(5)	88.4(2)–91.3(3)	91.0(1)–92.2(1)	88.2(4)–92.0(4)
$O_{oxime}LnO_{oxime}$	70.01(3)–72.73(4)	70.5(2)–74.2(2)	68.30(7)–69.51(6)	70.6(3)–73.4(3)

[a] Ligand = NO_3; [b] OAc; [c] lactate.

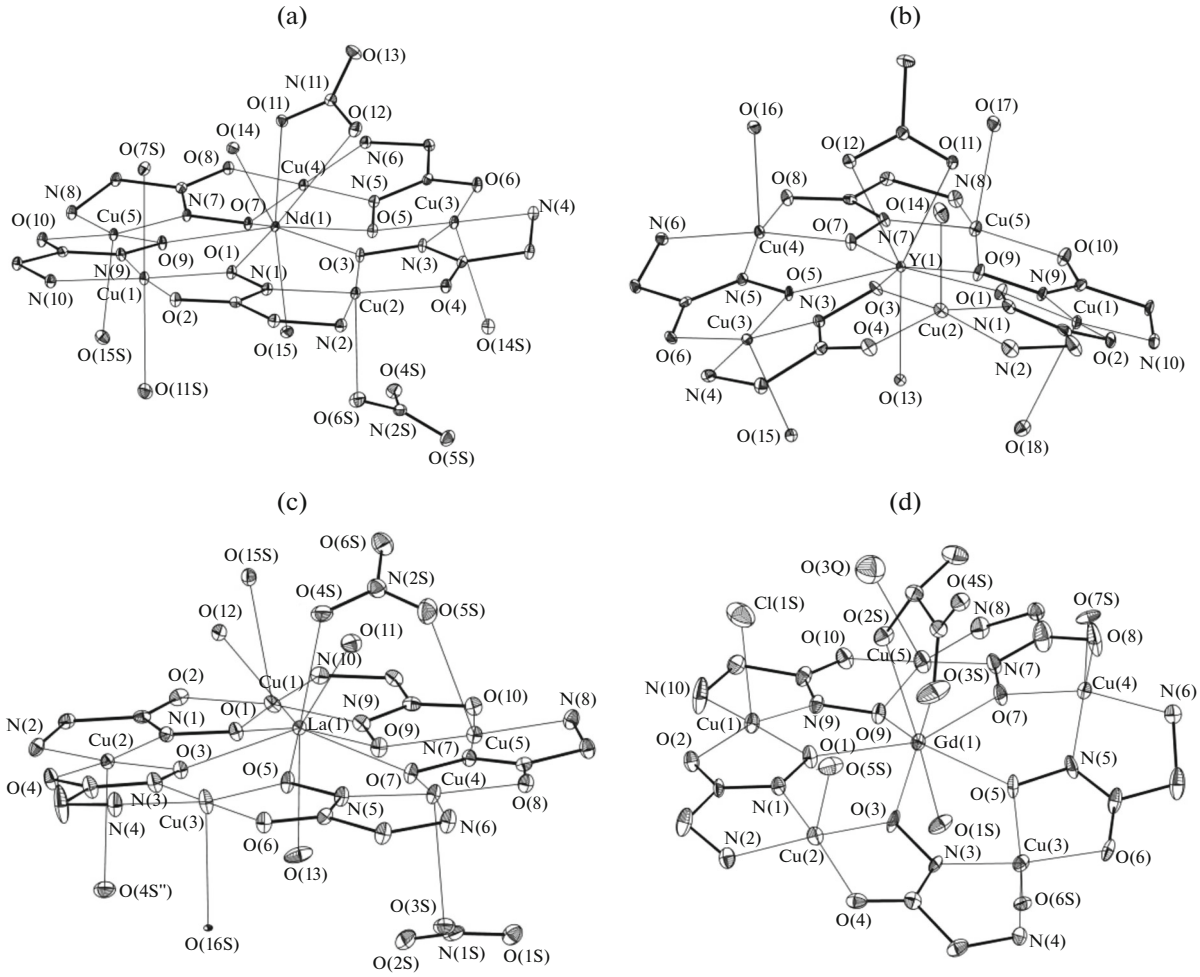

Fig. 5. Molecular structure of complexes (a) **III**, (b) **IV**, (c) **V**, and (d) **VI**.

Formally, the above-described complexes can be conceived as monoaqua (**I**, **II**, **IV**, and **VI**), diaqua (**III**), and triaqua (**V**) lanthanide compounds that may be potentially suitable as contrast agents. The detected trends of formation of the polynuclear metallacyclic complexes based on glycine hydroxamic acid with various anions coordinated to the central lanthanide ion allowed us to develop an original synthetic approach to tetraaqua complexes Ln[15-MC-5] [19]. The tetraaqua complexes, $Ln(H_2O)_4[15\text{-}MC_{Cu(II)Glyha}\text{-}5](Cl)_3$, were synthesized for the first time from $LnCl_3$, $Cu(CH_3COO)_2$, and glycine hydroxamic acid as the starting reactants without nitrate anions (Fig. 6). In the absence of nitrate anions, water is the major competitor (preferred over the acetate and chloride) for a coordination site at the lanthanide ion. All of the compounds $Ln(H_2O)_4[15\text{-}MC_{Cu(II)Glyha}\text{-}5]Cl$ (Ln = La (**VII**), Ce (**VIII**), Pr (**IX**), Nd (**X**), Sm (**XI**), Eu (**XII**), Gd (**XIII**), Tb (**XIV**), Dy (**XV**), Ho (**XVI**), Er (**XVII**), and Tm (**XVIII**)) are air-stable and readily water-soluble [19, 20].

The crystal structures were solved for compounds **VIII** and **XIII**, which are isostructural (Table 3). According to X-ray diffraction data, the Ln(III) atom is located at the center of the $15\text{-}MC_{Cu(II)Glyha}\text{-}5$ ring and is coordinated by five oxygen atoms, O(1), O(3), O(5), O(7), and O(9), in the equatorial plane and by four oxygen atoms of water, O(11)–O(14), in the apical position, which is significant for MRI contrasting. Three water molecules with the O(12)–O(14) atoms are located on one side and the fourth one (with O(11) atom) is on the opposite side (Fig. 7a). The Ln–$O(H_2O)$ distances somewhat differ, being in the range of 2.534(3)–2.622(3) Å. Four Cu(II) atoms are also coordinated to water molecules located on the same side as the three Ln(III)-coordinated water molecules. The Cu(4) atom is coordinated to Cl^-. The non-hydrogen atoms of the $15\text{-}MC_{Cu(II)Glyha}\text{-}5$ ring in **XIII** deviate from the plane by 0.21 Å. The deviation of the Gd atom in **XIII** from the metallamacrocycle plane towards three coordinated water molecules is 0.865 Å.

A specific feature of supramolecular structures of the tetraaqua complexes is the formation of numerous

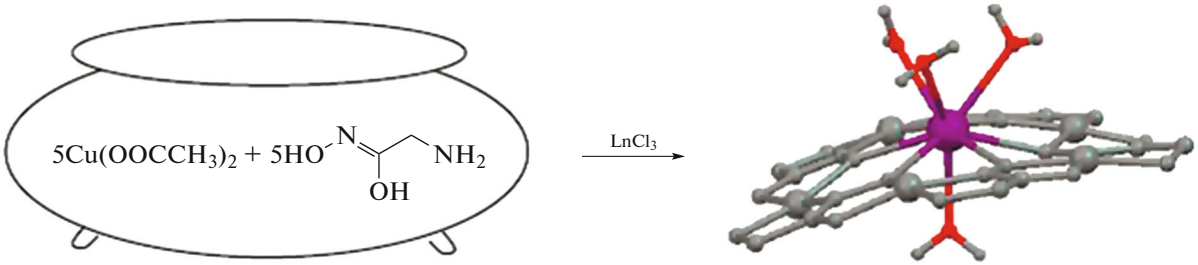

Fig. 6. Scheme of the synthesis of tetraaqua compounds $Ln(H_2O)_4$[15- $MC_{Cu(II)Glyha}$-5]Cl_3.

intermolecular bonds. Indeed, even in the crystalline state, compound **XIII** contains 14 water molecules per metallamacrocycle, and hydrogen bonds in **XIII** form a dense coil in which the distances between the water molecules and the 15-MC-5 ring ($H_w\cdots O_{MC}/O_w\cdots H_{MC}$) are in the 1.80–2.70 Å range. Figure 7b shows the short contacts and hydrogen bonds in complex **XIII**.

Note that functionalization of the metallamacrocycle organic ligand can not only change the efficiency and selectivity of ligand binding to the Ln^{3+} ion, but also give rise to more diverse molecular structures that may substantially differ in the properties. Optimization of the one-step method that we developed for the synthesis of tetraaqua complexes (Fig. 8) resulted in the synthesis of new water-soluble polynuclear Cu(II)-Ln(III) metallamacrocyclic complexes based on R-amino hydroxamic acids (R = alanine, phenylalanine, and tyrosine): $Ln(H_2O)_4$[15-$MC_{CuAlaha}$-5]Cl_3 (Ln = La (**XIX**), Ce (**XX**)); $Ln(H_2O)_3$[15-$MC_{CuPheha}$-5]Cl_3 (Ln = Ce (**XXI**), Gd (**XXII**)); $Ln(H_2O)_3$[15-$MC_{CuTyrha}$-5]Cl_3 (Ln = Gd (**XXIII**)) [21, 22]. As shown in the scheme (Fig. 8), chiral α-isomers of amino hydroxamic acids were used as the starting reactants, which gave rise to chiral polynuclear metallamacrocyclic derivatives. Comparison of the structural parameters of compounds **XIX**, **XXII**, and **XXIII** is presented in Table 4.

The bond lengths and angles of the inner metallamacrocycle are in the range usual for the Cu(II)-Ln(III) 15-MC-5 derivatives. A specific feature of the considered compounds is the position of R substituents relative to the inner metallamacrocycle, namely, they are all located on one side of the ring. However, the methyl substituents in **XIX** are situated on the same side as the three (or two, depending on the coordination number of the central lanthanide atom) water molecules coordinated to Ln(III). Meanwhile, the aromatic $-CH_2Ph$ and $-CH_2C_6H_4OH$ substituents in **XX**–**XXIII** point towards one Ln(III)-coordinated water molecule on the other side of the ring plane (thus forming a hydrophobic cavity).

The packing of dimeric molecules **XXI** and **XXII** in the crystal deserves special attention. As shown in Fig. 9, the crystal of **XXII** has two independent molecules (A and B), which differ in the coordination envi-

Table 3. Selected bond lengths (Å) and angles (deg) in compounds **VIII** and **XIII**

Bonds and angles	**VIII** (Ln = Ce)	**XIII** (Ln = Gd)
Cu–Ln	3.910(6)–4.056(6)	3.9089(5)–4.0560(5)
Cu–Cu	4.578(8)–4.610(8)	4.5741(7)–4.6107(7)
$Ln–O_{oxime}$	2.478(2)–2.570(2)	2.473(3)–2.567(3)
$Cu–O_{oxime}$	1.924(3)–1.943(2)	1.928(3)–1.944(3)
$Cu–O_{carbonyl}$	1.947(2)–1.955(3)	1.946(3)–1.957(3)
$Cu–N_{imine}$	1.902(3)–1.930(3)	1.905(3)–1.929(3)
$Cu–N_{amine}$	1.993(5)–2.031(3)	2.005(4)–2.023(3)
$Cu–O_{aq}$	2.3623(7)–2.4234(8)	2.369(3)–2.417(4)
Cu–Cl	2.6965(9)	2.699(1)
$Ln–O_{aq}$	2.5436(9)–2.6352(9)	2.534(3)–2.622(3)
$O_{oxime}CuN_{imine}$	89.31(12)–93.18(12)	89.4(1)–92.8(1)
$O_{oxime}LnO_{oxime}$	67.51(8)–72.69(8)	67.74(9)–72.76(9)

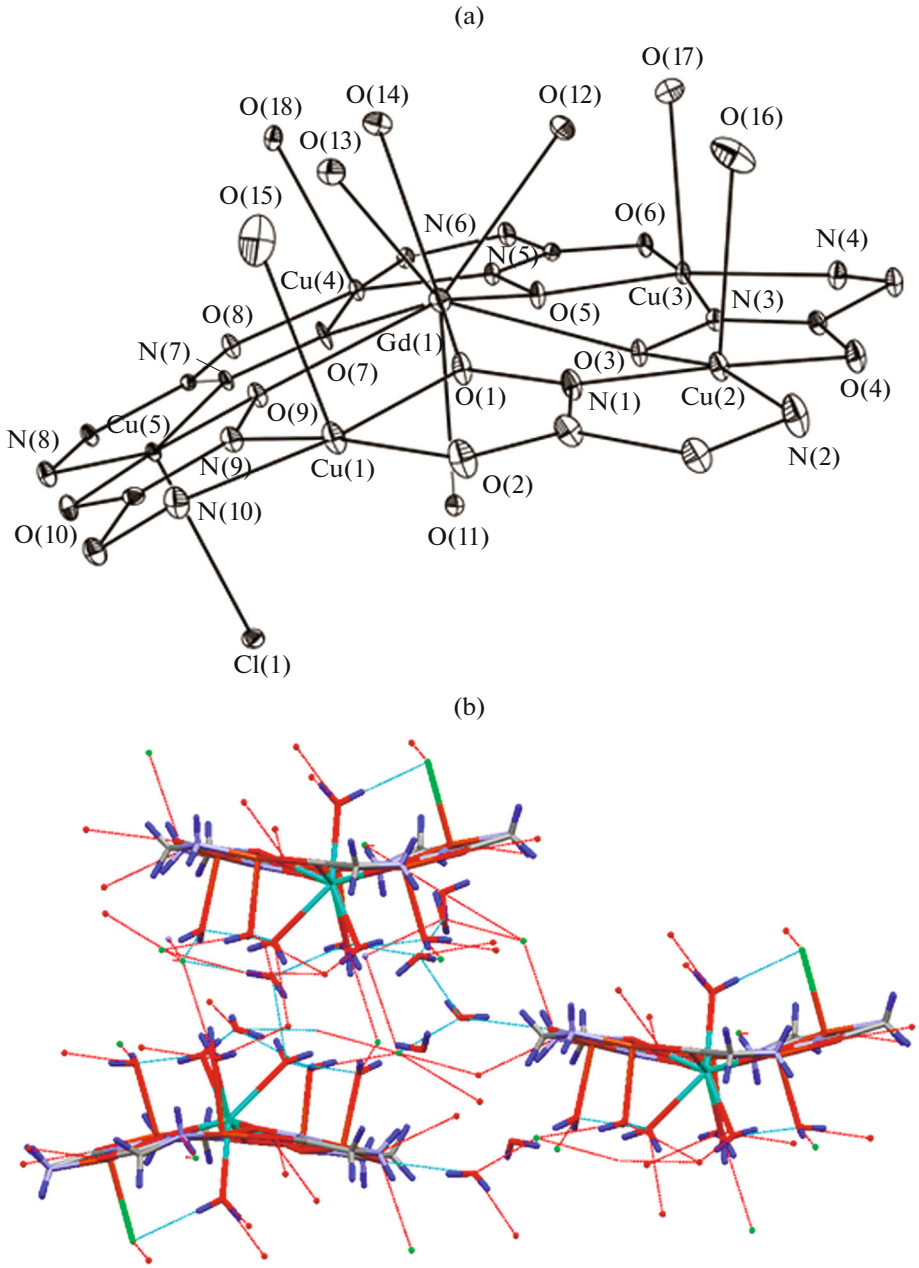

Fig. 7. (a) Molecular structure and (b) fragment of molecular packing of Gd(III) tetraaqua complex (**XIII**).

ronment of Cu(II). In molecule A, the Cu(II) atoms have 4 and 4 + 1 types of coordination, while all three types of Cu(II) coordination, 4, 4 + 1, and 4 + 2, are encountered in molecule B. In molecule A, only one Cl^- ion is coordinated to the Cu(2) atom, while in molecule B, two Cl^- anions are coordinated to the Cu(8) and Cu(10) atoms on the opposite sides of the metallacrown plane. The crystal of **XXI** contains two independent moieties with identical geometric parameters (Fig. 10). The Cu(1) and Cu(10) atoms have coordination number 4 + 2, while the other atoms have coordination number 4 + 1. A distinctive feature of **XXI** is the presence of a chloride bridge between Cu(3) and Cu(8) atoms (Cu–Cl, 2.671(8) and 2.661(7) Å), which combines the two moieties to form a "jaw" type sandwich structure filled by water molecules and chloride ions. This "jaw" is additionally stabilized by $Cl^-\cdots H_2O$ and $HOH\cdots OH_2$ hydrogen bonds, their lengths being comparable with the Ce–$O(H_2O)$ and Cu–$O(H_2O)$ distances.

A large number of intermolecular contacts and A–H···B hydrogen bonds with H···B distances of 2.06–3.39 Å are present.

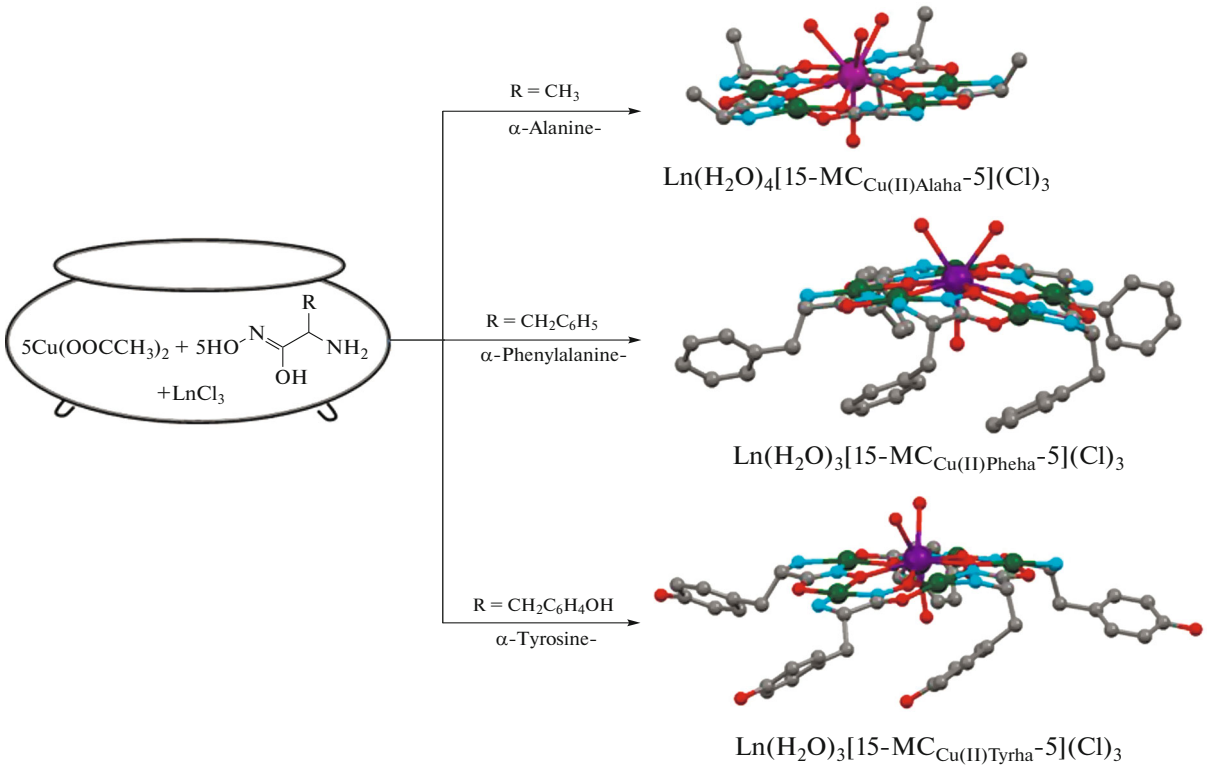

Fig. 8. Scheme of the synthesis of Cu(II)-Ln(III) metallamacrocyclic complexes based on R-amino hydroxamic acids.

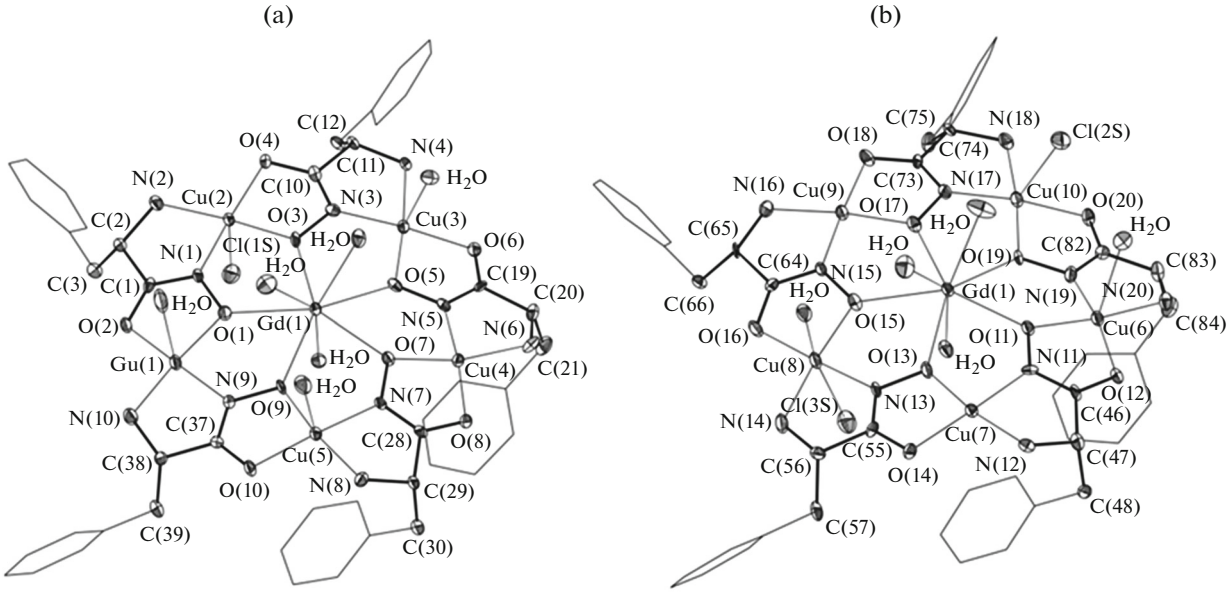

Fig. 9. Structure of two independent moieties (A and B) of compound **XXII**.

POLYNUCLEAR COPPER(II) AND LANTHANIDE(III) METALLAMACROCYCLIC COMPOUNDS AS POTENTIAL CONTRAST AGENTS FOR NMR STUDIES

A specific feature of the compounds in question is the presence of paramagnetic copper(II) and lanthanide(III) atoms, which markedly complicates ^{1}H NMR measurements. The ^{1}H NMR spectra of glycine hydroxamate complexes **VII**–**XV** in D_2O exhibit only one broad signal of the ligand α-proton in the 28.5–35 ppm range. This spectral pattern corresponds to pseudo-five-fold molecular symmetry observed for

Table 4. Comparison of structural parameters for **XIX**, **XXII**, and **XXIII**

Bonds and angles	**XIX** (Ln = La, R = Me)	**XXII** (Ln = Gd, R = CH_2Ph)	**XXIII** (Ln = Gd, R = $CH_2C_6H_4OH$)
$Ln–O_{oxime}$	2.514(6)–2.570(5)	2.373(9)–2.467(9)[a] 2.389(9)–2.432(9)[b]	2.388(10)–2.449(8)
$Cu–O_{oxime}$	1.900(6)–1.928(6)	1.913(8)–1.946(9)[a] 1.902(9)–1.955(8)[b]	1.912(9)–1.939(11)
$Cu–O_{carbonyl}$	1.923(6)–1.963(6)	1.891(9)–1.943(9)[a] 1.914(9)–1.938(9)[b]	1.884(13)–1.926(8)
$Cu–N_{imine}$	1.901(7)–1.912(7)	1.881(11)–1.921(11)[a] 1.874(10)–1.908(10)[b]	1.866(9)–1.894(12)
$Cu–N_{amine}$	1.980(8)–2.015(8)	1.991(11)–2.009(11)[a] 1.995(13)–2.025(11)[b]	1.997(12)–2.038(13)
$Cu–O_{aq}$	2.477(8)–2.85(1)	2.38(1)–2.64(1)[a] 2.48(1)–2.56(4)[b]	2.54(2)
$Ln–O_{aq}$	2.559(6)–2.633(6)	2.373(9)–2.469(9)[a] 2.364(9)–2.474(10)[b]	2.381(9)–2.55(4)
$O_{oxime}CuN_{imine}$	90.8(3)–92.6(3)	90.0(4)–91.8(4)[a] 90.1(4)–92.1(4)[b]	90.3(4)–91.5(4)
$O_{oxime}LnO_{oxime}$	67.73(19)–69.87(18)	70.1(3)–73.1(3)[a] 71.0(3)–73.2(3)[b]	70.5(3)–71.9(3)

[a] Geometric parameters corresponding to molecule A of **XXII**; [b] geometric parameters corresponding to molecule B of **XXII**.

15-MC-5 [23–26]. It is expedient to address the introduction of lactate into the metallacrown molecule (in relation to compound **VI** considered above) from the standpoint of application of these compounds as paramagnetic shift reagents for NMR measurements. Note that lactate determination is of prime importance for the diagnosis of a number of diseases such as cancer, diabetes, blood-stroke, and heart diseases [27]. The Ln(lactate)[15-$MC_{Cu(II)Glyha}$-5]$(Cl)_2$ lactate derivatives (Ln = La (**XXIV**), Ce (**XXV**), Pr (**XXVI**), Nd (**XXVII**), Sm (**XXVIII**), Eu (**XXIX**), Tb (**XXX**), and Dy (**XXXI**)), similar to the Gd complex (**VI**), were additionally synthesized for NMR measurements [18].

The total paramagnetic contribution of the metallacrown consists of two components related to coupling between the paramagnetic Cu^{2+} ions (antiferromagnetic) and between the paramagnetic central Ln^{3+} ion and Cu^{2+} ions (ferromagnetic) [11]. In order to isolate the paramagnetic contribution from copper ions, we studied the lanthanum complex **XXIV**, because La(III) is diamagnetic. The chemical shift difference between complexes **XXV**–**XXXI** with paramagnetic lanthanides (Ce, Pr, Nd, Sm, Eu, Tb, and Dy) and diamagnetic **LaXXIV** reflects the additional paramagnetic contribution from the Ln^{3+} ion (Table 5).

The results presented in Table 5 indicate that in terms of the paramagnetic contribution, the lanthanide complexes can be classified into two groups, one comprising Ce (**XXV**), Pr (**XXVI**), and Sm (**XXVIII**) complexes with a positive shift $\Delta\delta^{La}$ to higher frequency and the other comprising Eu (**XXIX**), Tb (**XXX**), and Dy (**XXXI**) complexes with a negative shift $\Delta\delta^{La}$ to lower frequency; the Nd compound (**XXVII**) showed a positive $\Delta\delta^{La1}$ shift of the H-methine proton

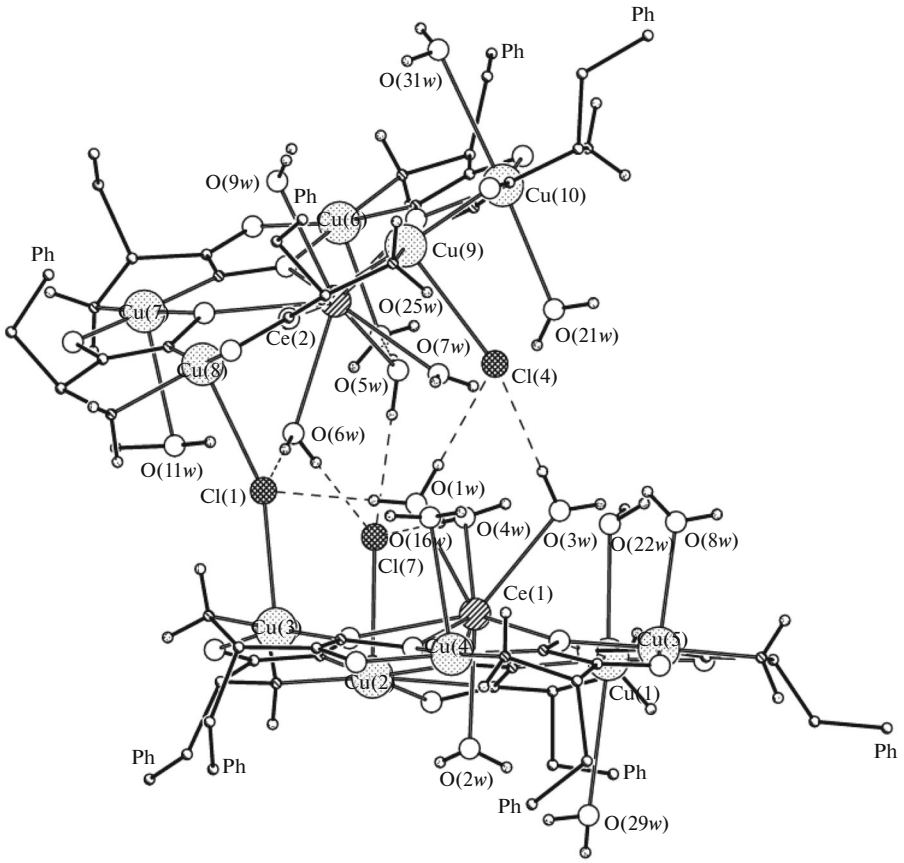

Fig. 10. General view of **XXI** with a jaw type sandwich structure.

Table 5. Chemical shifts of lactate CH and Me groups (δ), peak width at half height ($\nu_{1/2}$(Me or CH)), difference between the chemical shifts of **XXV**–**XXXI** and **XXIV** ($\Delta\delta^{La}$), and peak width at half height for water protons ($\nu_{1/2}(H_2O)$)

Compound	Ln	δ(Me)/$\nu_{1/2}$, ppm/Hz	δ(CH)/$\nu_{1/2}$, ppm/Hz	$\Delta\delta^{La}$(Me), ppm	$\Delta\delta^{La}$(CH), ppm	$\nu_{1/2}(H_2O)$, Hz
XXIV	La	2.18/69	4.61/73			10
XXV	Ce	2.74/78	5.72/78	+0.56	+1.11	30
XXVI	Pr	2.84/73	5.8/88	+0.66	+1.19	8.5
XXVII	Nd	1.97/73	5.91/89	–0.21	+1.3	5
XXVIII	Sm	2.31/76	4.61/75	+0.13	0	8
XXIX	Eu	1.96/72	3.8/72	–0.22	–0.81	13
VI	Gd	2.18/(>500)	4.61/(>500)	0	0	71
XXX	Tb	2.0/45	3.92/53	–0.18	–0.69	15
XXXI	Dy	2.11/(>400)	4.23/(>400)	–0.07	–0.38	57

and a negative $\Delta\delta^{La1}$ shift of the H-methyl proton. These data are inconsistent with the Bleaney's theory of magnetic anisotropy and belong to the class of exceptions for low-symmetry paramagnetic lanthanide coordination compounds described in [28]. Note that the best relationship between the chemical shift amplitude and the line width was found for the Pr (**XXVI**) and Nd (**XXVII**) complexes. In the case of Gd (**VI**), the widest signal was observed in comparison with those of complexes **XXV**–**XXXI**. The NMR line width is known to correspond to the relaxation times T_1 and T_2. The wider the lines, the shorter these times and the higher the relaxation values r_1 and r_2, which are characteristic parameters of magnetic resonance imaging contrast agents.

The interest in the development of a new class of contrast agents for high-field MRI is related to the modern use of high-field (above 3 T) systems. High-field magnets provide a better quality of the image, accelerated scanning, and a wider scope of applicability. This technique makes it possible to reveal almost faultlessly ischemic, hemorrhagic, and mixed types of stroke and microstroke. Meanwhile, it is noteworthy that the efficiency of classical contrast agents substantially decreases with increasing field strength; as a result, the known clinical contrast agents do not meet the requirements of high-field MRI [29]. A traditional solution to this problem is attempt to increase the number of coordinated water molecules (q) to two, because for classical contrast agents, $q = 1$ (Fig. 11). According to the Solomon–Blombergen–Morgan (SBM) theory, the parameter q is one of the factors determining the relaxation value [30].

An advantage of the considered polynuclear metallamacrocyclic compounds over the classical contrast agents is the rigidity of the metallacrown frame and the open coordination sphere of the lanthanide atom in the apical direction, which resulted in the number of coordinated water molecules up to $q = 4$ (**VII**–**XVIII**). The relaxation analysis of the tetraaqua complexes $Ln(H_2O)_4[15\text{-}MC_{Cu(II)Glyha}\text{-}5](Cl)_3$ (**VII**–**XVIII**) was carried out on a high-field magnetic resonance scanner (9.4 T) at 18°C. The results of measurements of the spin–lattice r_1 and spin–spin r_2 relaxations of the tetraaqua complexes $Ln(H_2O)_4[15\text{-}MC_{Cu(II)Glyha}\text{-}5](Cl)_3$ are summarized in Table 6 [19].

The gadolinium tetraaqua complex **XIII** showed the highest relaxation characteristics among the lanthanide complexes and, moreover, the characteristics are more than twice higher than those of the commercial Magnevist contrast agent ($r_1 = 4.8$ mM^{-1} s^{-1}, $r_2 = 4.4$ mM^{-1} s^{-1} (at 9.4 T) [31]). The relaxation characteristics of the La complex **VII** (caused by the paramagnetic effect of copper ions) are insignificant. The highest paramagnetic effect of the Gd^{3+} ion is attributed to its unique symmetrical ground state with a half-filled shell. Note that lanthanide ions such as Tb^{3+}, Dy^{3+}, Ho^{3+}, and Er^{3+} have high magnetic moments (9.7, 10.6, 10.6, 10.4, and 9.6 μ_B, respectively) as compared with the Gd^{3+} ion (7.9 μ_B), but asymmetry of the electronic states of these ions results in a very fast electron relaxation, which in turn leads to a considerable decrease in the r_1 and r_2 values [32].

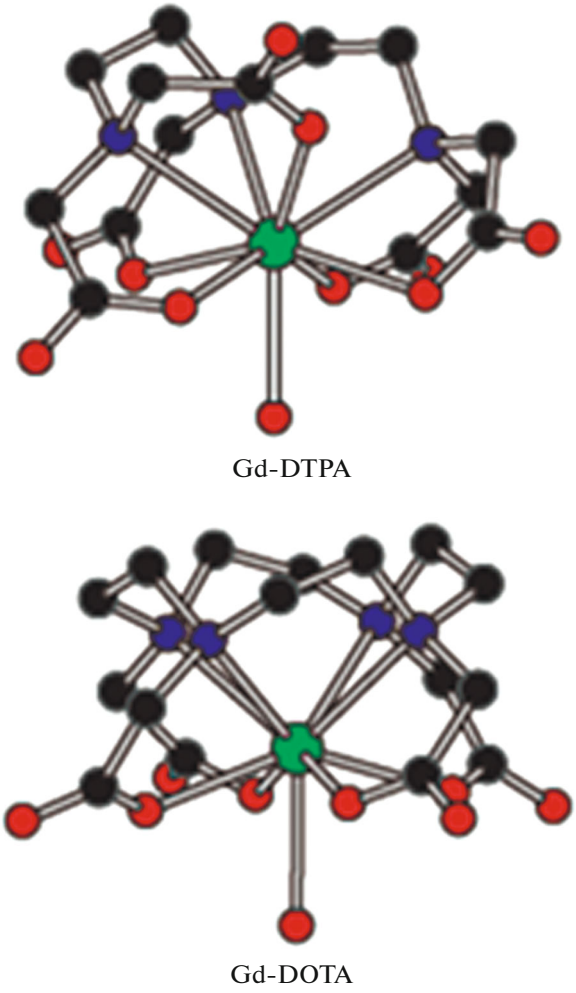

Fig. 11. Structure of classical contrast agents Gd-DPTA (Magnevist) and Gd-DOTA ($q = 1$).

Complex **XIII** was tested as a contrast agent on the local ischemia of the rat brain motor cortex [33]. Figure 12 illustrates the accumulation of the new complex in the ischemic area, which is accompanied by increase in the intensity at the site. The accumulation of the contrast agent was monitored for 30 min after its intravenous injection. The highest intensity at the site was observed 20 min after the intravenous injection of the agent. The acute toxicity experiments of the complex were carried out on sexually mature white noninbred mice (5 males) and rats (5 males). The animals administered with equivalent amounts of physiological saline (5 males) served as the control. The experiment showed a 100% survival of the animals upon sin-

Table 6. Relaxation values for $Ln(H_2O)_4$[15-$MC_{Cu(II)Glyha}$-5]$(Cl)_3$ (9.4 *T*, 18°C)

Compound	Ln	r_1, s^{-1} mM^{-1}	r_2, s^{-1} mM^{-1}
VII	La	0.17	0.56
VIII	Ce	0.18	0.12
IX	Pr	0.11	0.27
X	Nd	0.20	0.23
XI	Sm	0.10	0.36
XII	Eu	0.35	0.09
XIII	**Gd**	**11.46**	**11.60**
XIV	Tb	0.66	0.59
XV	Dy	0.83	1.96
XVI	Ho	0.81	0.82
XVII	Er	0.80	0.58
XVIII	Tm	0.58	0.43

gle-shot intravenous injection of complex **XIII** with a concentration of 0.5 mmol/mL in a dose of 0.1 mmol per kg for mice and 0.3 mmol per kg for rats. During the experiment, the behavior and appearance of animals were monitored for 14 days. No deviations from the norm were detected after the agent administration.

POLYNUCLEAR COPPER(II) AND LANTHANIDE(III) METALLAMACROCYCLIC COMPOUNDS AS NEW MOLECULAR PRECURSORS OF NANOSTRUCTURED MATERIALS

The presented polynuclear compounds with a 5 : 1 copper to lanthanide stoichiometric ratio are of obvious interest for their use as single source molecular precursors for the synthesis of nano-sized inorganic materials of particular composition and structure.

The thermal behavior of the complexes $Ln(H_2O)_4$[15-$MC_{CuGlyha}$-5]Cl_3 (**VII**–**XV**), $Ln(H_2O)_4$-[15-$MC_{CuAlaha}$-5]Cl_3 (**XX**), and $Ln(H_2O)_3$[15-$MC_{CuPheha}$-5]Cl_3 (**XXI**) was studied in a nitrogen atmosphere by thermogravimetric analysis combined with mass spectrometric determination of the composition of various products of thermolysis, and differential scanning calorimetry. The studies demonstrated that in the 40–150°C range, all complexes undergo stepwise destructive changes of the same type [34]. Figure 13 shows the temperature dependences of the mass change, the rate of mass change, and heat flux for Ce(III) complexes **VIII**, **XX**, and **XXI**. The first step of decomposition occurs in the temperature range of 40–150°C and is accompanied by an endothermic effect. The mass spectrum of the gas phase in the 40–150°C range corresponds to the spectrum of H_2O. On further heating, the obtained solid products are stable up to ~180°C, then the major mass loss stage occurs in the range of 190–250°C, being accompanied by a considerable exothermic effect. A specific feature of decomposition of metallacrowns in this stage is the formation of the corresponding lanthanide oxides, together with the destruction of the organic part of the molecule; therefore, the temperatures of the exothermic stage differ considerably depending on the nature of the central lanthanide atom (Fig. 14).

It is noteworthy that the mass spectra of the complexes in the temperature range of 190–600°C show ions corresponding to the H_2O and CO_2 molecules, nitroxide (NO^+) and/or formaldehyde ($H_2C{=}O$), and cyanic (HOCN) and isocyanic acids (H–N=C=O), which attests to destruction of the amino hydroxamate ligands. Among the products of incomplete thermal decomposition of metallacrown **XX**, when using the procedure reported in [18] in the presence of calcium acetate, we isolated a complex containing CN groups. According to X-ray diffraction data, the obtained complex Nd(OAc)[15-$MC_{Cu(II)Glyha}$-5]$(Cl)_{2.5}$Ca-$(OH)_{0.5}$(CN) crystallizes in space group $P\bar{1}$ (Fig. 15). The neodymium atom is located at the centre of the metallacrown ring and is bound to five oxygen atoms of 15-$MC_{Cu(II)Glyha}$-5, two oxygen atoms of the acetate ligand, and two oxygen atoms of water molecules. The

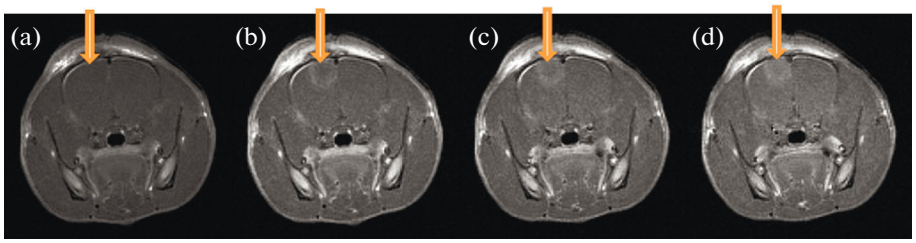

Fig. 12. T1-weighed images of rat brain with ischemic stroke site: (a) before introduction of the contrast complex, (b) immediately after intravenous injection of contrast complex **XIII**, (c) 10 min after introduction of the complex, (d) 10–20 min after the introduction of the complex.

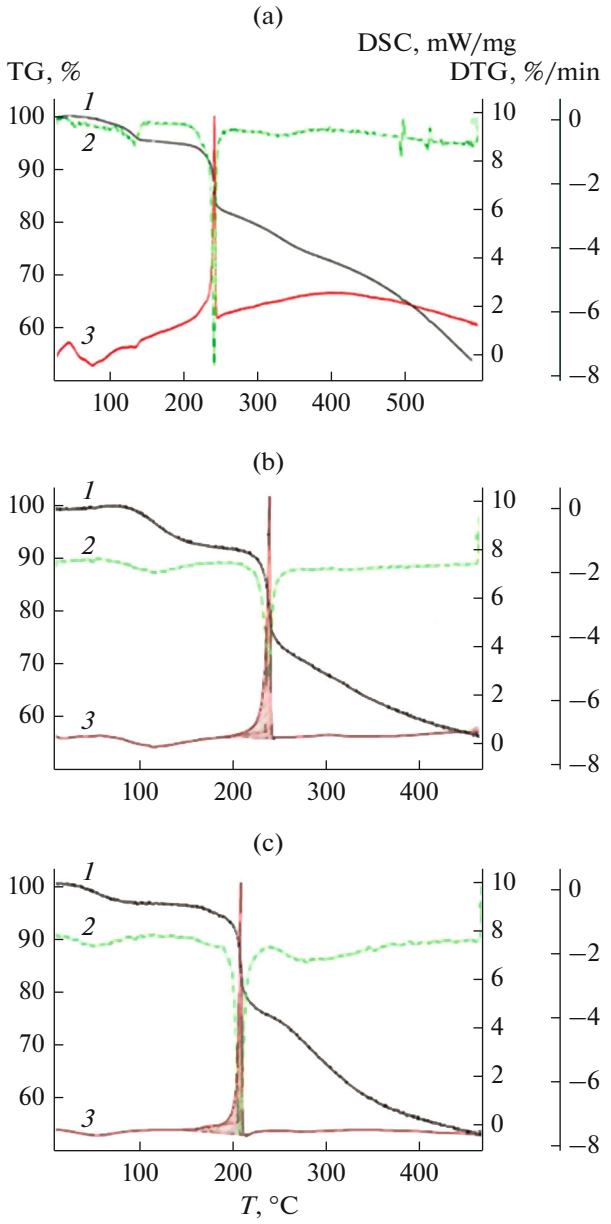

Fig. 13. (*1*) Mass change, (2) rate of mass change, and (*3*) heat flux vs. temperature for complexes (a) **VIII**, (b) **XX**, and (c) **XXI**.

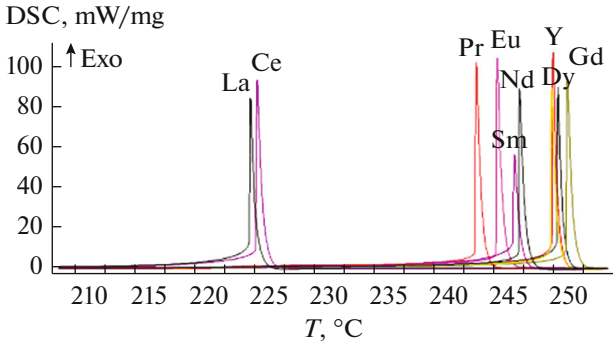

Fig. 14. DSC curves for $Ln(H_2O)_4$[15-$MC_{CuGlyha}$-5]Cl_3 (**VII**–**XV**), N_2, 5 K/min.

coordination environment of Ca^{2+} in the structure is disordered over two positions in 1 : 1 ratio; calcium is bound to one chlorine atom and to either OH^- oxygen or CN^- nitrogen.

On the basis of the obtained results and published data on thermal decomposition of hydroxamic acids [1, 35], a scheme of thermolysis was proposed, including, on the one hand, oxidation (accompanied by reduction of Cu^{2+}) of the amine group ($-CH_2-NH_2$) to the nitrile group ($-C\equiv N$) and, on the other hand, the formation of an isocyanate group upon the Lossen rearrangement. The processes related to the formation of structures of the final solid decomposition products are completed at a much higher temperature. According to powder X-ray diffraction, the final solid decomposition products are copper and lanthanide oxides.

The Ce(III) complexes **VIII**, **XX**, and **XXI** were tested as molecular precursors of nanostructured materials. The optimal conditions were found for the hydrothermal synthesis of a Ce/Cu nanomaterial based on multiwalled carbon nanotubes (MWCNTs) (Fig. 16).

The hybrid nanomaterials based on MWCNTs and nanostructured cerium and copper oxides attract considerable attention of chemists and physicists, owing to their unique properties in combination with low cost. They cover a broad range of potential applications in catalysis, the design of sensors, and energy saving devices. Hydrothermal synthesis is considered to be promising for the fabrication of these hybrid systems. A significant obstacle for the manufacture of uniform coatings on the hydrophobic MWCNT surface is that carbon nanotubes are prone to stick together. The pristine MWCNTs are agglomerates of nanotubes, that is, entangled coils of various size in which hundreds of carbon nanotubes are held together by van der Waals forces. It is well known that surfactants and ultrasonic treatment are often used for the preparation of homogeneous dispersions of MWCNTs. However, the presence of surfactants often deteriorates the properties of hybrid nanomaterials; therefore, currently, procedures using ultrasonic treatment receive much attention.

In order to attain a uniform distribution of metal-containing species on the MWCNT surface under hydrothermal conditions, an attempt was made to form a uniform MWCNT suspension in aqueous solutions of complexes **VIII**, **XX**, and **XXI**. The addition of metallamacrocyclic complexes **VIII**, **XX**, and **XXI**, differing by the substituents in the metallacrown ring (R = H, Me, and CH_2Ph, respectively), considerably increases the stability of aqueous dispersions of

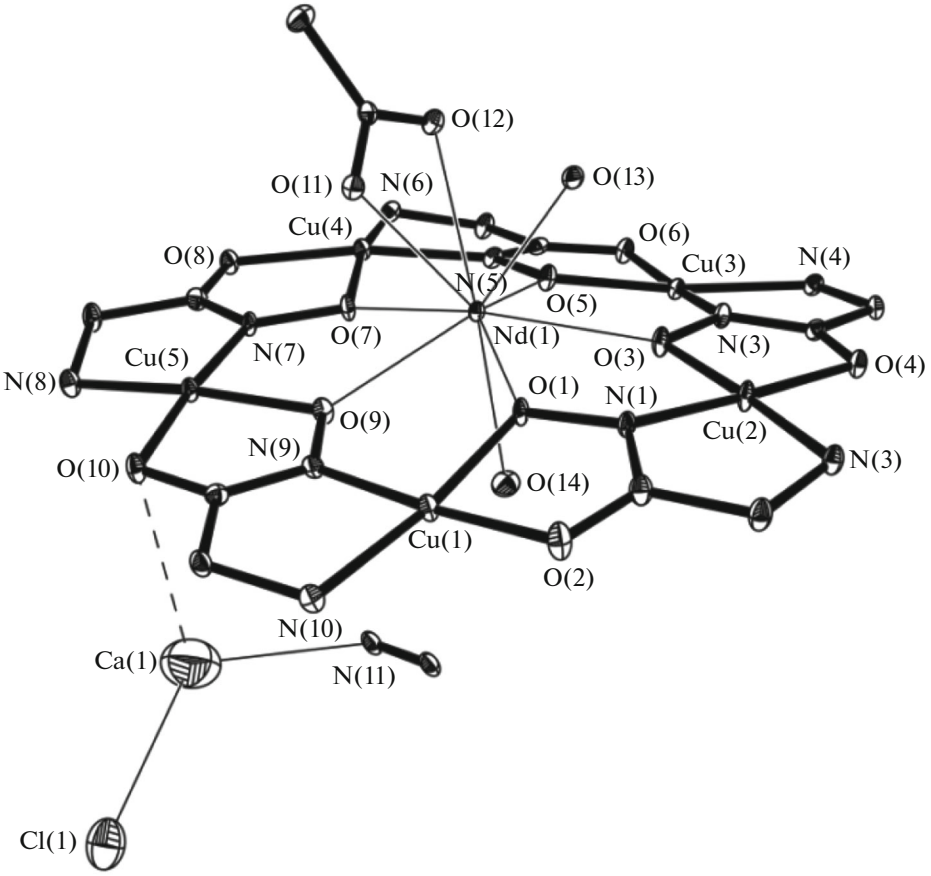

Fig. 15. Molecular structure of Nd(OAc)[15-$MC_{Cu(II)Glyha}$-5]$(Cl)_{2.5}Ca(OH)_{0.5}(CN)$.

Fig. 16. Scheme of the hydrothermal synthesis of hybrid materials based on metallacrowns and MWCNTs.

MWCNTs, indicating the possibility of using them as precursors for hydrothermal synthesis without surfactants. The aqueous dispersion of **XXI**/MWCNTs (Fig. 17) was the most stable. From the time dependences of the precipitation efficiency of dispersions of (**VIII**, **XX**, and **XXI**)/MWCNTs presented in Fig. 18, one can see that **XXI**/MWCNTs shows the lowest precipitation efficiency as compared with **VIII**/MWCNTs or **XX**/MWCNTs. Indeed, even when an aqueous dispersion of **XXI**/MWCNTs is allowed to stand for 180 h, only approximately 20% of MWCNTs precipitate. This effect is obviously attributable to

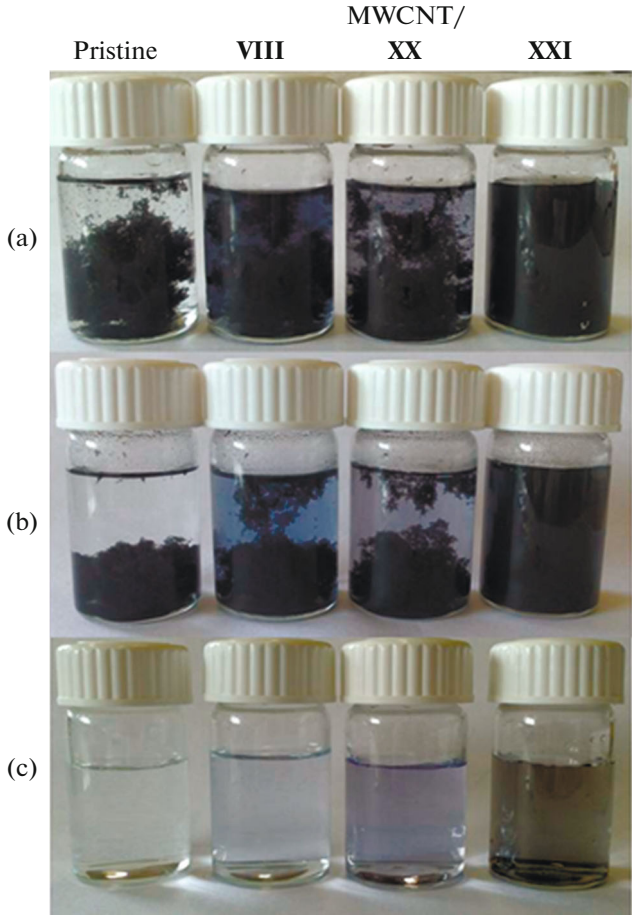

Fig. 17. Photo images of aqueous dispersions of pristine MWCNTs and (**VIII**, **XX**, **XXI**)/MWCNTs obtained (a) immediately after ultrasonic treatment, (b) after 30 days of standing, and (c) after centrifugation for 20 min at 6000 rpm.

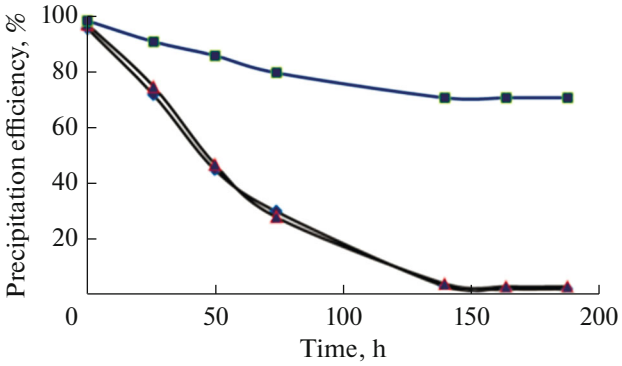

Fig. 18. Efficiency of precipitation of aqueous dispersions of MWCNTs in the presence of complexes (◆) **VIII**, (▲) **XX**, and (■) **XXI**.

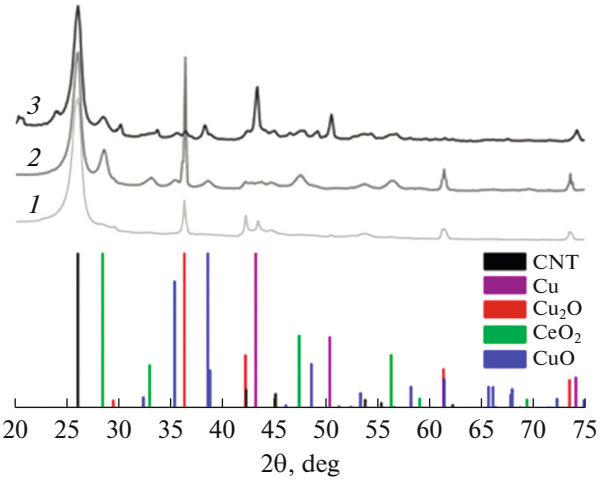

Fig. 19. X-ray diffraction patterns of the products of hydrothermal treatment of aqueous dispersions of (*1*) **VIII**/MWCNTs, (*2*) **XX**/MWCNTs, (*3*) **XXI**/MWCNTs.

additional non-covalent π–π-interaction between the MWCNT surface and the ligand phenyl groups in **XXI**.

According to powder X-ray diffraction, the solid products formed upon hydrothermal treatment of aqueous dispersions of (**VIII**, **XX**, **XXI**)/MWCNTs include in all cases MWCNTs, CeO_2, Cu, Cu_2O, and CuO (Fig. 19). The crystallite sizes (nm) are as follows: Cu, ~30–40; Cu_2O, ~45–50; CuO and CeO_2, ~15–20. The hybrid materials thus formed were studied by scanning electron microscopy (SEM) and energy dispersive X-ray spectroscopy (EDS). The SEM images of hybrid materials obtained from the aqueous dispersions of **VIII**, **XX**, and **XXI**/MWCNTs are shown in Fig. 20. Unlike **VIII**/MWCNTs and **XX**/MWCNTs, in the case of **XXI**/MWCNTs, the distribution of the nanostructured phases over the MWCNT surface is much more uniform, which is accompanied by better dispersion properties of **XXI** containing phenylalanine groups.

A study of the morphology of the metal-containing hybrid materials (**VIII**, **XX**, **XXI**)/MWCNTs has shown that the crystallites on MWCNTs form mesocrystals shaped as porous spheres 250–300 nm in diameter, petals arranged as 300–400 nm flowers, or well-faceted mesocrystals, for example, cubes (Fig. 21). The mesocrystals, so-called superstructures formed by self-assembly of crystallites, or non-classical crystals, are know to represent a special type of materials with a specific self-assembling hierarchical structure.

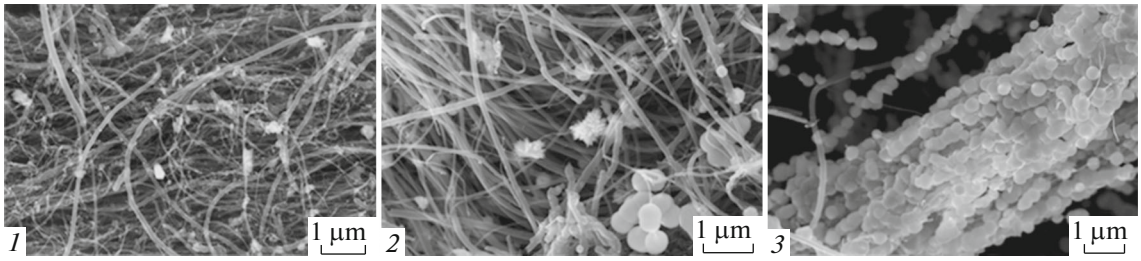

Fig. 20. SEM images of the hybrid material obtained from aqueous dispersions of (*1*) **VIII**/MWCNTs, (*2*) **XX**/MWCNTs, and (*3*) **XXI**/MWCNTs.

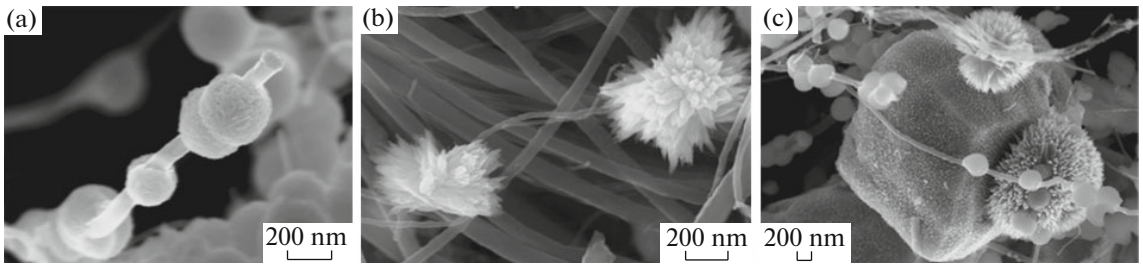

Fig. 21. SEM images of the hybrid material obtained from aqueous dispersions of (**VIII**, **XX**, **XXI**)/MWCNTs: (a) spherical mesocrystals, (b) flow-like mesocrystals, (c) well faceted mesocrystals.

ACKNOWLEDGMENTS

This work was partly supported by the Russian Foundation for Basic Research, project 15-43-02285 r_povolzh'e_a).

REFERENCES

1. Marmion, C.J., Griffith, D., and Nolan, K.B., *Eur. J. Inorg. Chem.,* 2004, vol. 2004, p. 3003.
2. Kurzak, B., Kozlowski, H., and Farkas, E., *Coord. Chem. Rev.*, 1992, vol. 114, p. 169.
3. Gupta, S.P., *Chem. Rev.*, 2015, vol. 115, p. 6427.
4. Ford, P., *Chem. Sci.*, 2016, vol. 7, p. 2964.
5. Solomon, E.I., Heppner, D.E., Johnston, E.M., et al., *Chem. Rev.*, 2014, vol. 114, p. 3659.
6. Sidorov, A.A., Kiskin, M.A., Aleksandrov, G.G., et al., *Russ. J. Coord. Chem.*, 2016, vol. 42, p. 581.
7. Mezei, G., Zaleski, C.M., and Pecoraro, V.L., *Chem. Rev.*, 2007, vol. 107, p. 4933.
8. Tegoni, M. and Remelli, M., *Coord. Chem. Rev.*, 2012, vol. 256, p. 289.
9. Bodwin, J.J., Cutland, A.D., Malkani, R.G., et al., *Coord. Chem. Rev.*, 2001, vols. 216–217, p. 489.
10. Lah, M.S. and Pecoraro, V.L., *J. Am. Chem. Soc.*, 1989, vol. 111, p. 7258.
11. Stemmler, A.J., Kampf, J.W., Kirk, M.L., et al., *Inorg. Chem.*, 1999, vol. 38, p. 2807.
12. Cutland, A.D., Malkani, R.G., Kampf, J.W., et al., *Angew. Chem., Int. Ed. Engl.*, 2000, vol. 39, p. 2689.
13. Lim, C.S., Kampf, J.W., and Pecoraro, V.L., *Inorg. Chem.*, 2009, vol. 48, p. 5224.
14. Tegoni, M., Tropiano, M., and Marchio, L., *Dalton Trans.*, 2009, p. 6705.
15. Jankolovits, J., Lim, C.S., Mezei, G., et al., *Inorg. Chem.*, 2012, vol. 51, p. 4527.
16. Pavlishchuk, A.V., Kolotilov, S.V., Fritsky, I.O., et al., *Acta Crystallogr., Sect. C: Cryst Struct. Commun.*, 2011, vol. 67, p. m255.
17. Katkova, M.A., Zabrodina, G.S., Muravyeva, M.S., et al., *Inorg. Chem. Commun.*, 2015, vol. 52, p. 31.
18. Katkova, M.A., Zabrodina, G.S., Muravyeva, M.S., et al., *Eur. J. Inorg. Chem.*, 2015, vol. 2015, p. 5202.
19. Muravyeva, M.S., Zabrodina, G.S., Samsonov, M.A., et al., *Polyhedron*, 2016, vol. 114, p. 165.
20. Kremlev, K.V., Samsonov, M.A., Zabrodina, G.S., et al., *Polyhedron*, 2016, vol. 114, p. 96.
21. Katkova, M.A., Zabrodina, G.S., Kremlev, K.V., et al., *Mendeleev Commun.*, 2017, vol. 27, p. 402.
22. Katkova, M.A., Zabrodina, G.S., Kremlev, K.V., et al., *Thin Solid Films*, 2017, vol. 628, p. 112.
23. Parac-Vogt, T.N., Pacco, A., Nockemann, P., et al., *Eur. J. Inorg. Chem.*, 2006, vol. 2006, p. 1466.
24. Pacco, A., Parac-Vogt, T.N., van Besien, E., et al., *Eur. J. Inorg. Chem.*, 2005, vol. 2005, p. 3303.
25. Jankolovits, J., Kampf, J.W., and Pecoraro, V.L., *Inorg. Chem.*, 2013, vol. 52, p. 5063.
26. Parac-Vogt, T.N., Pacco, A., Nockemann, P., et al., *Chem.-Eur. J.*, 2006, vol. 12, p. 204.

27. Adeva-Andany, M., Lopez-Ojen, M., Funcasta-Calderon, R., et al., *Mitochondrion*, 2014, vol. 17, p. 76.

28. Funk, A.M., Finney, K.N.A., Harvey, P., et al., *Chem. Sci. J.*, 2015, vol. 6, p. 1655.

29. Caravan, P., Farrar, C.T., Frullano, L., et al., *Contrast. Media Mol. Imaging*, 2009, vol. 4, p. 89.

30. Caravan, P., *Chem. Soc. Rev.*, 2006, vol. 35, p. 512.

31. Watanabe, T., Frahm, J., and Michaelis, T., *Brain Struct. Funct.*, 2015, vol. 220, p. 1529.

32. Caravan, P., Ellison, J.J., McMurry, T.J., et al., *Chem. Rev.*, 1999, vol. 99, p. 2293.

33. Murav'eva, M.S., Klyuev, E.A., Katkova, M.A., et al., *Vest. SPb Gos. Univ. Ser. 4*, 2016, vol. 3, no. 61, p. 70.

34. Makarov, S.G., Zabrodina, G.S., Cherkasov, A.V., et al., *Macroheterocycles*, 2016, vol. 9, p. 263.

35. Hassner, A. and Stumer, C., *Organic Syntheses Based on Name Reactions and Unnamed Reactions*, Oxford: Elsevier, 1994.

Translated by Z. Svitanko